




Role of Jakob number in Leidenfrost phenomena unveiled by theoretical modeling

Cite as: Phys. Fluids **31**, 042109 (2019); <https://doi.org/10.1063/1.5082266>

Submitted: 20 November 2018 . Accepted: 26 March 2019 . Published Online: 23 April 2019

Meng Shi (史萌), Felix Frank , Letian Wang (王乐天) , Feng Xu (徐峰), Tian Jian Lu (卢天健), and Costas P. Grigoropoulos 



View Online



Export Citation



CrossMark

ARTICLES YOU MAY BE INTERESTED IN

[Self-propelled rotation of paper-based Leidenfrost rotor](#)

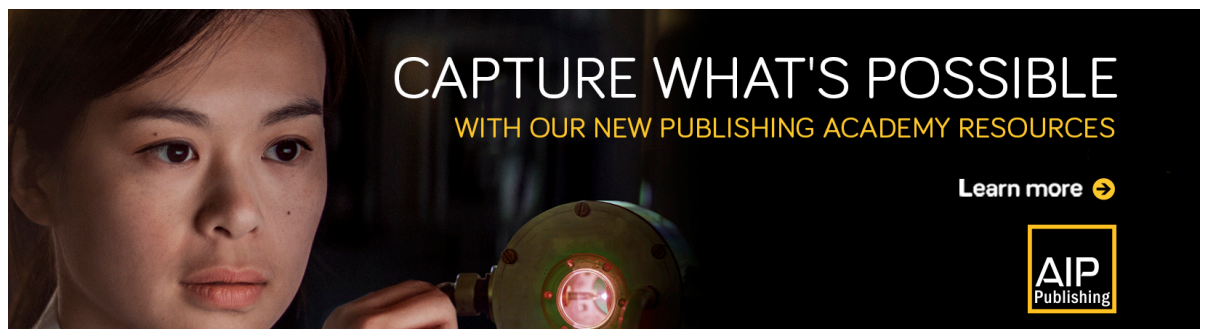
Applied Physics Letters **114**, 113703 (2019); <https://doi.org/10.1063/1.5084231>

[Leidenfrost drops](#)


Physics of Fluids **15**, 1632 (2003); <https://doi.org/10.1063/1.1572161>



[Bubble interactions and bursting behaviors near a free surface](#)

Physics of Fluids **31**, 042104 (2019); <https://doi.org/10.1063/1.5088528>



CAPTURE WHAT'S POSSIBLE
WITH OUR NEW PUBLISHING ACADEMY RESOURCES

Learn more 



Role of Jakob number in Leidenfrost phenomena unveiled by theoretical modeling

Cite as: *Phys. Fluids* **31**, 042109 (2019); doi: [10.1063/1.5082266](https://doi.org/10.1063/1.5082266)

Submitted: 20 November 2018 • Accepted: 26 March 2019 •

Published Online: 23 April 2019



View Online



Export Citation



CrossMark

Meng Shi (史萌),^{1,2,3} Felix Frank,¹ Letian Wang (王乐天),¹ Feng Xu (徐峰),^{3,4} Tian Jian Lu (卢天健),^{5,6.a)} and Costas P. Grigoropoulos^{1,a)}

AFFILIATIONS

¹Laser Thermal Laboratory, Department of Mechanical Engineering, University of California, Berkeley, California 94720-1740, USA

²School of Energy and Power Engineering, Xi'an Jiaotong University, Xi'an 710049, People's Republic of China

³Bioinspired Engineering and Biomechanics Center (BEBC), Xi'an Jiaotong University, Xi'an 710049, People's Republic of China

⁴The Key Laboratory of Biomedical Information Engineering of Ministry of Education, School of Life Science and Technology, Xi'an Jiaotong University, Xi'an 710049, People's Republic of China

⁵State Key Laboratory of Mechanics and Control of Mechanical Structures, Nanjing University of Aeronautics and Astronautics, Nanjing 210016, People's Republic of China

⁶Nanjing Center for Multifunctional Lightweight Materials and Structures (MLMS), Nanjing University of Aeronautics and Astronautics, Nanjing 210016, People's Republic of China

^{a)}Authors to whom correspondence should be addressed: cgrigoro@berkeley.edu and tjlu@nuaa.edu.cn

ABSTRACT

The Leidenfrost phenomenon in its most common form is encountered when a droplet is levitated and driven by its own vapor. The recently discovered “cold Leidenfrost phenomenon” expands this phenomenon into low-temperature regimes. Although various theoretical models have been proposed, analytical exploration on generalized dimensionless laws is still absent. In this work, we elucidated the role of the dimensionless Jakob number in the Leidenfrost phenomenon through theoretical modeling. The model was verified by examining the cold Leidenfrost phenomenon of both a dry ice nub on the surface of water and a liquid nitrogen droplet on a smooth silicon surface. Regardless of the specific configuration, the dimensionless temperature distribution in the vapor film only depends on the Jakob number of the vapor and presents linear dependence when the Jakob number is below 0.25. This theoretical model would facilitate the exploration of physics for Leidenfrost events and, therefore, guide prediction as well as the design of applications in the future.

Published under license by AIP Publishing. <https://doi.org/10.1063/1.5082266>

I. INTRODUCTION

The Leidenfrost phenomenon,¹ wherein a droplet is levitated and driven by its own vapor when placed on a superheated surface, was first reported in 1756 and has been developed into diverse manifestations and applications.^{2–10} For instance, a self-propelled Leidenfrost droplet was demonstrated on a 460 °C ratchet-like microstructure,⁴ which opens a door to develop a self-powered fluidic device through the Leidenfrost phenomenon. Afterward, a “Leidenfrost cart” was developed to realize frictionless transportation on a teeth-shaped surface at 355 °C.³ Furthermore, the Leidenfrost phenomena have been extended to solids.^{6,11} A “Leidenfrost engine” was designed to generate electricity through the motion of a dry ice nub on a hot turbine-like structure (500 °C).¹¹ On the other hand, based

on the overheated and charged status of the Leidenfrost droplet during fast evaporation, it was used to synthesize gold nanoparticles as a chemical reactor¹² and to identify chemical species.¹³ With the rapid development of nanofabrication, more and more novel activities based on Leidenfrost phenomena were performed on the nanostructures.^{14–20} Nevertheless, these Leidenfrost systems are associated with the limitation of the requirement for high temperatures to generate evaporated gas.

Recently, “cold Leidenfrost phenomena” have been designed, targeting a broader range of applications.^{21–24} For instance, a levitated and self-propelled acetone droplet in a Leidenfrost state was found on hot water substrates (65 °C), and the miscible droplet can even bounce off the substrate if the impact velocity is high enough.²⁴ Furthermore, a room temperature (20 °C) Leidenfrost water droplet

was achieved through reducing the environmental pressure around the droplet, and the droplet can have a spontaneous trampoline behavior with potential application for energy conversion.²³ At even lower temperature ($-78.5\text{ }^{\circ}\text{C}$), a self-propelled hovercraft was developed by placing a dry ice device on the room temperature water, which enables a novel way to utilize programmable self-propelled devices over the water surface.²¹ Interestingly, a water droplet could also be levitated and bounce on a piece of dry ice through the substrate's sublimation, which provides an alternative approach to achieve "water repellence."²⁵ At extreme temperature ($-196\text{ }^{\circ}\text{C}$), an aqueous droplet was found to be levitated on liquid nitrogen, which has great importance for droplet cryopreservation.^{22,26}

Theoretical models have been established to investigate various Leidenfrost phenomena.^{2,27-34} The classical one could be traced back to 1966, when an analytical model of the Leidenfrost phenomenon was postulated to illustrate the film boiling behavior of droplets with spheroid shape, which revealed that the major contribution to the heat transfer in the Leidenfrost phenomenon is the convective conduction.¹ Afterward, the approximate Leidenfrost droplet model of the heat and mass balance through the vapor film provided a convenient way to predict the film thickness underneath the droplet.²⁷ By solving the Young-Laplace equation, a mathematic model for the Leidenfrost effect with precise droplet geometry was developed, which implied that the calculation in Leidenfrost problem may be reduced to the solution of three first-order ordinary differential equations.²⁸ At the same time, the theoretical models also helped to investigate the motion behaviors of an object (droplet or solid) in a Leidenfrost system. To explain the directional movement of uneven dry ice in a Leidenfrost state, the Leidenfrost phenomenon of the dry ice levitated on the hot surface was theoretically analyzed and it was found that asymmetric mass distributions in a Leidenfrost solid can lead to a nonhomogeneous vapor flow and thus generate a lateral force.² To illustrate the self-propulsion principle of a droplet on a surface with a temperature gradient, a model of a Leidenfrost droplet on a hot surface with a temperature gradient was developed and it was surprisingly found that the variability of vapor properties

with temperature is instrumental for the droplet to move.³¹ Recently, the Navier slip model for drag reduction by the Leidenfrost phenomenon was developed, which provides a simple one parameter characterization of the drag reduction phenomenon due to a stable vapor layer.³² However, these models are usually established for specific cases, and there is still a lack of an analytical exploration on common dimensionless laws for Leidenfrost phenomena.

Examination and comparison of reported studies show that Leidenfrost phenomena share the common physics in that the generated vapor provides levitation. Therefore, herein, we developed a comprehensive theoretical model for Leidenfrost phenomena highlighting the important role of the Jakob number (defined as the ratio of the sensible heat of vapor to the latent heat of evaporation). The physics studied involve the fully coupled heat and mass transfer, fluid mechanics, and force balance. This model yielded the analytical solutions of vapor film thickness underneath the object, as well as the velocity, pressure, and temperature distributions. The respective theoretical results for the evaporation rate of dry ice and mass variation of liquid nitrogen droplet were verified by experimental results. The crucial role of the Jakob number in temperature distribution was revealed. This theoretical model provides an efficient way to explore the physics of Leidenfrost events conveniently, hence guiding prediction as well as the design of new variations and applications in the future.

II. THEORETICAL MODELING

The classical Leidenfrost phenomenon refers to a water droplet levitated by the vapor film produced as a result of the heat transfer between the droplet and the heated surface¹ [Fig. 1(a)]. On the other hand, in the Leidenfrost phenomenon of dry ice on water, the dry ice is levitated by the vapor film generated by its sublimation²¹ [Fig. 1(b)]. Similarly, a liquid nitrogen droplet on a room temperature surface is levitated by the vapor film evaporated from the droplet that is heated by the surface;⁴ and an aqueous droplet on

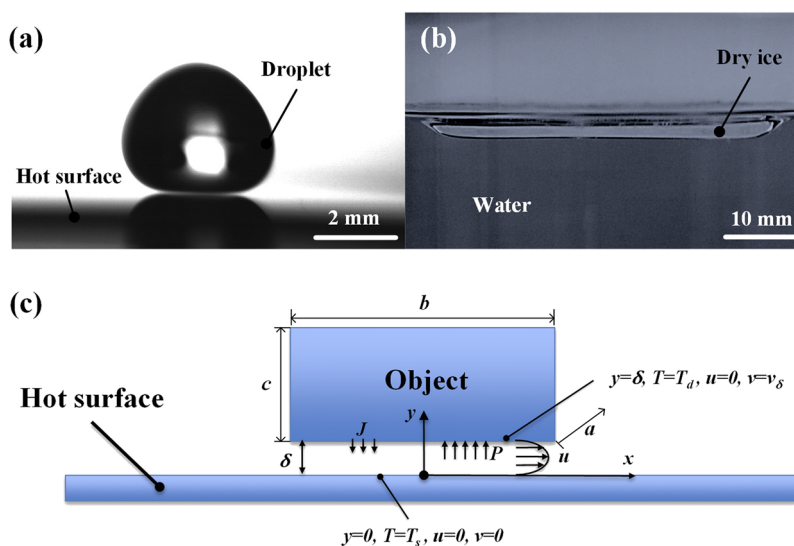


FIG. 1. Theoretical sketch and various pictures of the Leidenfrost phenomenon: (a) water droplet levitated over a $300\text{ }^{\circ}\text{C}$ hot surface, (b) dry ice hovercraft on the room temperature water surface, and (c) theoretical sketch of the Leidenfrost phenomenon geometry examined in this work.

the surface of liquid nitrogen is levitated by the vapor film from the evaporation of liquid nitrogen.^{22,26}

Regardless of whether the vapor comes from the object or the substrate and whether they are liquid or solid, the Leidenfrost phenomenon happens as long as the vapor produced can provide a sufficient levitation force. Evidently, the vapor film underneath the droplet plays a key role in the Leidenfrost phenomenon. Due to the large temperature difference and extremely thin vapor film between the object and substrate, the heat transfer and the temperature gradient in the normal direction across the vapor film are much higher than in the tangential direction.

Based on the above summary, we utilized a two-dimensional geometric configuration for the Leidenfrost phenomenon system [Fig. 1(c)]. To simplify the analysis and explore the dominant physics, the vapor film underneath the object was assumed to be of uniform thickness since it is sufficiently thin compared with the characteristic length of object (typical orders of magnitude are $10^2 \mu\text{m}$ for the film thickness and a few millimeters for the object length²). For investigating the flow behavior in the vapor film, the lubrication analysis was utilized since the thickness of vapor film ($\sim \mu\text{m}$) is much smaller than its length ($\sim \text{mm}$) and the vapor flow can be treated as laminar due to its sufficiently small Reynold number (typically of the order of 1).¹ Based on the lubrication analysis, the continuity equation and Navier-Stokes equations can be simplified as

$$\frac{\partial u}{\partial x} + \frac{\partial v}{\partial y} = 0, \tag{1}$$

$$\frac{\partial P}{\partial x} = \mu \frac{\partial^2 u}{\partial y^2}, \tag{2}$$

$$\frac{\partial P}{\partial y} = 0. \tag{3}$$

In Eqs. (1)–(3), u (m/s) and v (m/s) are the parallel and vertical velocities of vapor flow, respectively, P (Pa) is the pressure in the vapor film, μ (Pa s) is the viscosity of the vapor, x and y are the dimensional variables in the parallel and the vertical direction, respectively. As argued earlier, the heat transfer in the vertical direction is much higher than in the parallel direction; hence, the energy conservation equation in the quasisteady state can be written as

$$v \frac{\partial T}{\partial y} = \alpha \frac{\partial^2 T}{\partial y^2}, \tag{4}$$

where T (K) is the temperature. α (m^2/s) is the thermal diffusivity of the vapor which satisfies $\alpha = k/(\rho_v c_p)$, and k [$\text{W}/(\text{m K})$], ρ_v (kg/m^3), and c_p [$\text{J}/(\text{kg K})$] are the thermal conductivity, density, and specific heat of the vapor, respectively. For simplification, we regarded the vapor as Newtonian and no-slip boundary conditions that were assumed. Thus, the boundary conditions of these equations can be expressed as

$$y = 0, \quad u = 0, \quad v = 0, \quad T = T_s, \tag{5}$$

$$y = \delta, \quad u = 0, \quad v = v_\delta, \quad T = T_d, \tag{6}$$

where δ (m) is the thickness of the vapor film. T_s (K) and T_d (K) are the temperatures of the substrate and the object, respectively. v_δ (m/s) is the vertical vapor velocity at the bottom of object, which represents the velocity of produced vapor from the surface of the

object. Integrating Eq. (2) and applying the boundary conditions (5) and (6), the parallel velocity profile is derived,

$$u = \frac{1}{2\mu} \frac{\partial P}{\partial x} y(y - \delta). \tag{7}$$

Substituting Eq. (7) into (1), integrating, and applying boundary condition (5), we obtain the vertical velocity profile,

$$v(y) = -\frac{1}{2\mu} \frac{\partial^2 P}{\partial x^2} \left(\frac{1}{3} y^3 - \frac{1}{2} \delta y^2 \right). \tag{8}$$

Thus,

$$v_\delta = v(\delta) = \frac{\delta^3}{12\mu} \frac{\partial^2 P}{\partial x^2}. \tag{9}$$

The energy balance equation at the interface of the levitated object and vapor can be expressed as

$$JL = \rho_v v_\delta L = k \left. \frac{\partial T}{\partial y} \right|_{y=\delta}, \tag{10}$$

where J [$\text{kg}/(\text{m}^2 \text{s})$] is the mass flux of vapor flow and L (J/kg) is the latent heat of evaporation. $(\partial T/\partial y)_{y=\delta}$ represents the thermal gradient at the interface of object and vapor. Substituting Eq. (10) into (9), and combining with Eq. (8), we obtain

$$v(y) = -\frac{6k}{\rho_v L \delta^3} \left. \frac{\partial T}{\partial y} \right|_{y=\delta} \left(\frac{1}{3} y^3 - \frac{1}{2} \delta y^2 \right). \tag{11}$$

Substituting into Eq. (4),

$$\left(-\frac{6k}{\rho_v L \delta^3} \left. \frac{\partial T}{\partial y} \right|_{y=\delta} \left(\frac{1}{3} y^3 - \frac{1}{2} \delta y^2 \right) \right) \frac{\partial T}{\partial y} = \alpha \frac{\partial^2 T}{\partial y^2}. \tag{12}$$

Thus, the heat transfer profile across the vapor film can be quantified by solving differential Eq. (12) and applying the boundary conditions (5) and (6),

$$T(y) = \frac{T_d - T_s}{\int_0^\delta e^{-\frac{k}{\rho_v L \delta^3} \left. \frac{\partial T}{\partial y} \right|_{y=\delta} \left(\frac{1}{2} y^4 - \delta y^3 \right)} dy} \int_0^y e^{-\frac{k}{\rho_v L \delta^3} \left. \frac{\partial T}{\partial y} \right|_{y=\delta} \left(\frac{1}{2} y^4 - \delta y^3 \right)} dy + T_s. \tag{13}$$

We nondimensionalized Eq. (13)

$$y = \delta y^*, \tag{14}$$

$$T = T_s + (T_d - T_s) T^*, \tag{15}$$

$$Ja = \frac{c_p (T_s - T_d)}{L}, \tag{16}$$

where y^* and T^* are the dimensionless length and temperature, respectively. Ja is the Jakob number, defined as the ratio of sensible heat of vapor to latent heat of evaporation. Thus,

$$T^*(y) = \frac{1}{\int_0^1 Ja \left. \frac{\partial T^*}{\partial y^*} \right|_{y^*=1} \left(\frac{1}{2} (y^*)^4 - (y^*)^3 \right) dy^*} \int_0^{y^*} e^{Ja \left. \frac{\partial T^*}{\partial y^*} \right|_{y^*=1} \left(\frac{1}{2} (y^*)^4 - (y^*)^3 \right)} dy^*. \tag{17}$$

The thermal gradient at $y = \delta$ is equal to

$$\left. \frac{\partial T^*}{\partial y^*} \right|_{y=1} = \frac{1}{\int_0^1 e^{Ja \frac{\partial T^*}{\partial y^*} \Big|_{y=1} (\frac{1}{2}(y^*)^4 - (y^*)^3)} dy^*} e^{-\frac{1}{2} Ja \frac{\partial T^*}{\partial y^*} \Big|_{y=1}}. \quad (18)$$

Thus, the dimensionless thermal gradient can be determined by solving Eq. (18) and consequently, the dimensionless temperature is given by Eq. (17), with both only depending on the Jakob (Ja) number.

At the same time, the second derivative of pressure can be found via Eqs. (9) and (10),

$$\frac{\partial^2 P}{\partial x^2} = \frac{12\mu k}{\rho_v L \delta^3} \left. \frac{\partial T}{\partial y} \right|_{y=\delta}. \quad (19)$$

Because of the symmetry of the geometrical configuration, the first derivative of pressure at $x = 0$ is equal to zero, while the pressure at the boundary of the object ($x = b/2$) is atmospheric pressure [P_0 (Pa)]. Through the integration of Eq. (19), the expression of pressure distribution can be written as

$$P(x) = \frac{6\mu k}{\rho_v L \delta^3} \left. \frac{\partial T}{\partial y} \right|_{y=\delta} \left(x^2 - \left(\frac{b}{2} \right)^2 \right) + P_0. \quad (20)$$

Furthermore, the aggregate pressure-induced force must balance the weight of the object (W),

$$W = 2 \int_0^{b/2} P(x) adx - abP_0 = -\frac{\mu kab^3}{\rho_v L \delta^3} \left. \frac{\partial T}{\partial y} \right|_{y=\delta}. \quad (21)$$

In Eq. (21), W (N) is equal to $\rho_d V_d g$, where ρ_d (kg/m^3) and V_d (m^3) are the density and volume of the object, respectively, and g (m/s^2) is the gravitational acceleration constant. In the geometric configuration examined in this study, $V_d = abc$, and a , b , and c (m) are the length, width, and height of the object, respectively. Thus, we obtain

$$\left. \frac{\partial T}{\partial y} \right|_{y=\delta} = -\frac{c\rho_d g \rho_v L \delta^3}{\mu kb^2}. \quad (22)$$

Meanwhile, by using Eqs. (14) and (15),

$$\left. \frac{\partial T}{\partial y} \right|_{y=\delta} = \frac{T_d - T_s}{\delta} \left. \frac{\partial T^*}{\partial y^*} \right|_{y=1}. \quad (23)$$

Thus, the thickness (δ) of the vapor film can be determined by substituting Eq. (22) into (23),

$$\delta = \left(\frac{-\mu kb^2 (T_d - T_s)}{c\rho_d g \rho_v L} \left. \frac{\partial T^*}{\partial y^*} \right|_{y=1} \right)^{1/4}. \quad (24)$$

Since the dimensionless thermal gradient is solved via Eq. (18), the film thickness can be found from Eq. (24) and the thermal gradient obtained from Eq. (22). Therefore, the profiles of temperature (T), pressure (P), and vertical and parallel velocities (u and v) of the vapor can be determined.

To consider the time effect, we took account of the weight reduction by incorporating the evaporation of the object into the

model. Referring to Eqs. (10) and (23), the evaporation rate of the object can be written as

$$M_e = -Jab = -\frac{abk}{L} \left. \frac{\partial T}{\partial y} \right|_{y=\delta} = -\frac{abk}{L} \frac{T_d - T_s}{\delta} \left. \frac{\partial T^*}{\partial y^*} \right|_{y=1}. \quad (25)$$

Consequently, the weight of the evaporating object with respect to time [t (s)] is

$$W = \left(\rho_d V_d - \int_0^t M_e dt \right) g = \left(\rho_d V_d - \frac{abk(T_s - T_d)}{L} \left. \frac{\partial T^*}{\partial y^*} \right|_{y=1} \int_0^t \frac{1}{\delta} dt \right) g. \quad (26)$$

Substituting Eq. (26) into (21)–(23), the time-dependent film thickness is determined by solving the following equation:

$$\delta = \left(\left(\frac{\mu kb^2 (T_s - T_d)}{c\rho_d g \rho_v L} \left. \frac{\partial T^*}{\partial y^*} \right|_{y=1} \right)^{-3/4} - \frac{3\rho_v g}{4\mu b^2} t \right)^{-1/3}. \quad (27)$$

Thus, the velocity and pressure transient profiles can be determined via substituting Eq. (27) into Eqs. (22), (20), (11), and (7).

III. MODEL DEMONSTRATION AND EXPERIMENTAL VALIDATION

A. Leidenfrost phenomenon of dry ice on water surface

To demonstrate the predictive ability of the above theoretical model, the Leidenfrost phenomenon of a dry ice nub on the water was chosen as a representative example for calculations. This Leidenfrost phenomenon was observed when placing a dry ice device on the surface of room temperature water.²¹ Even the density of dry ice (1562 kg/m^3 , 25°C) is higher than that of water (998 kg/m^3 , 25°C), the dry ice device can be levitated on the water surface by the produced carbon dioxide vapor due to its sublimation. As an example, we calculated the physical profiles (including distribution of temperature, velocity, and pressure) of the Leidenfrost system of dry ice nubs (78.5°C) with dimensions of $50 \text{ mm} \times 10 \text{ mm} \times 3 \text{ mm}$ on the surface of water at room temperature (25°C). The results at the initial time ($t = 0$) are shown in Fig. 2. The evaporation rates of dry ice nubs on the water surface at different temperatures (from 18 to 32°C) were also accounted.

To obtain the temperature, pressure, velocity, and other physical profiles in the Leidenfrost phenomenon, the above equations were solved via computational software (Wolfram Mathematica 11). The Jakob number was calculated through Eq. (16), while the dimensionless temperature distribution can be easily assessed by Eq. (17). Hence, the evaporation rate and the film thickness can be obtained by Eqs. (25) and (27). To extend the analysis, the pressure profile, the parallel, and vertical velocity distribution can be achieved by Eqs. (20), (7), and (8), respectively. The total velocity profile can be calculated through combining parallel and vertical velocity. The Reynolds number (Re) was calculated as $Re = \rho_v u_{\max} \delta / \mu$, where u_{\max} is the maximum parallel velocity along the y axis.

To verify this theoretical work, experiments on the measurement of the dry ice evaporation rate on the water of different temperatures were performed. Dry ice nubs were formed in an aluminum

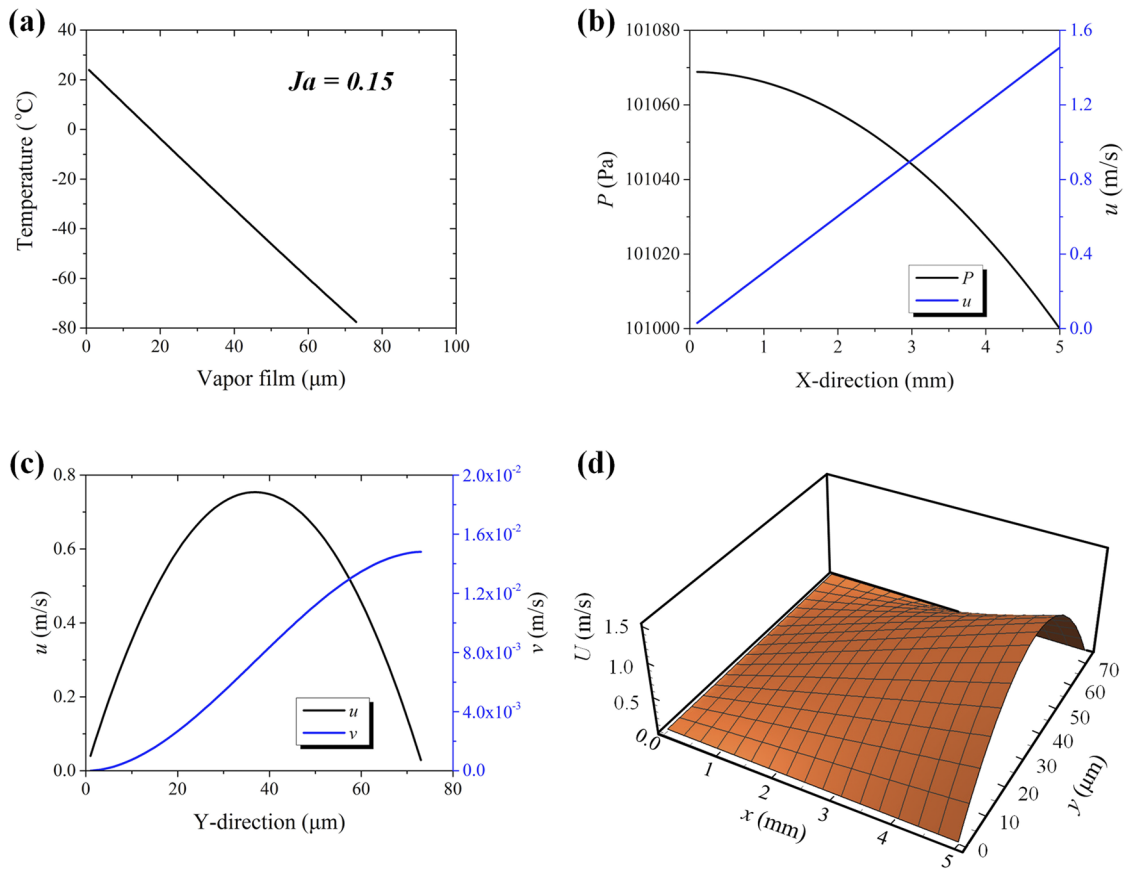


FIG. 2. Temperature, pressure, and velocity distribution in vapor film: (a) temperature distribution, (b) pressure and parallel velocity (u) in the X-direction, (c) parallel (u) and vertical velocity (v) in the vapor film (Y-direction), and (d) total vapor velocity (U) distribution in the vapor film.

module, with dimensions of 50 mm × 10 mm × 3 mm, and placed on the water surface. The length of dry ice nubs is intentionally much longer than the width and height to minimize three-dimensional effects. A 60 ml volume water was added into the 85 mm dish and placed on the scale. The temperature of water was monitored and measured using a K-type thermocouple. The water temperature was controlled and adjusted through replacing the cold water by hot water before every experiment. Since the heat capacity of water is high and each experiment was performed in a short time around 1 min, the temperature of the water pool is estimated to have limited variation (~3 °C).

The mass variation of the entire dish including the water and the dry ice inside during the initial 25 s was recorded using a digital camera off the scale readings. Since the evaporation of water can be ignored (experimental measurement: $\sim 4 \times 10^{-7}$ kg/s, from 18 to 32 °C), the mass variation of the entire dish (Δm_d , kg) can be regarded as the weight variation of the dry ice. Thus, the experimental evaporation rate of dry ice on the water can be calculated as

$$M_e = \frac{\Delta m_d}{\Delta t}, \tag{28}$$

where Δt (s) is the evaporation time recorded after placing the dry ice onto the water surface.

B. Leidenfrost phenomenon of liquid nitrogen droplet on smooth silicon surface

To demonstrate the importance of Jakob number with nonlinear temperature distribution, we also performed the experiments of liquid nitrogen (−196 °C) droplets on a smooth silicon surface at room temperature (22 °C). Since the heat capacity of nitrogen vapor and the vaporization latent heat of liquid nitrogen are 1040 J/(kg K) and 1.9875×10^5 J/kg, respectively, the Ja number of this phenomenon will be ~ 1.14 , which belongs to a nonlinear temperature distribution case. We measured the mass variation of a 0.05 g liquid nitrogen droplet on the smooth silicon surface at room temperature and compared with the theoretical mass variations as predicted by our model with nonlinear temperature and linear temperature hypothesis ($\nabla^2 T = 0$, commonly used in a previous model^{27,28,30,35}).

Before experiments, we first placed a 140 mm plastic dish on a scale, then, a 4-in. smooth silicon wafer was placed into the dish. A round gasket (outer diameter: 21 mm and inner diameter: 8 mm) was put on the center of silicon wafer to limit the motion area of liquid nitrogen droplets. After that, the display number on the scale was reset to zero. During experiments, we utilized a spoon to slightly add the liquid nitrogen droplets (around 0.06 g) into the gasket and

on the surface of silicon and we used a digital camera to record the variation of display number on the scale until the liquid nitrogen droplets evaporated out. After experiments, the videos were analyzed frame by frame to collect the data. To have a similar initial mass of liquid nitrogen droplets to compare with theoretical results, we started to collect the data when the mass of liquid nitrogen droplets is close to 0.05 g. We repeated the experiments more than 7 times, and each experiment started 3 min after the last one to let the silicon surface recover to room temperature ($\sim 22^\circ\text{C}$). The temperature of the silicon surface was monitored and measured using a K-type thermocouple.

The theoretical mass variations were calculated by our model with nonlinear temperature distribution [Eq. (17)] and linear temperature distribution hypothesis ($\nabla^2 T = 0$). For the nonlinear case, the temperature distribution was determined by Eq. (17) based on the Jakob number, and the dimensionless thermal gradient was determined by Eq. (18). Then, the transient film thickness can be calculated by Eq. (27), and thus, the evaporation rate [Eq. (25)] followed by the mass variation can be determined. For the linear case, the temperature distribution was determined by $\nabla^2 T = 0$, and the dimensionless thermal gradient will be equal to 1. The mass variation can be determined through similar methods as the nonlinear case. We approximate the droplet as a cubic shape with the same volume to simplify the calculation. In addition, a better geometric model and theoretical model will be developed in our future study.

IV. RESULTS

Before calculating the physical fields, we verified the validity of applying the lubrication approximation in this work. The Reynolds number (Re), film thickness, maximum parallel, and vertical velocity at the symmetry axis of the vapor film were calculated to be ~ 8.8 , 7.4×10^{-5} m, 1.5 m/s, and 0.015 m/s, respectively. Therefore, the vapor flow can be treated as laminar since the Reynolds number is very small, and the lubrication approximation can be used in this analysis since the film thickness is much smaller than the characteristic length of the object (~ 10 mm). On the other hand, the vertical velocity is much smaller than the parallel velocity.

Since the Leidenfrost phenomenon is driven by the temperature difference between the object and the surface, we first calculated the temperature distribution across the vapor film [Fig. 2(a)] that is nearly linear. Furthermore, the thermal gradient at the bottom of the object is high, at $\sim 1.34 \times 10^6$ K/m, since the thickness of the vapor film is small. We also calculated the parallel velocity at the center of the vapor film and the pressure distribution along the x-direction (u and P). The results indicated that the pressure decreased away from the symmetry axis, eventually reaching ambient pressure. The parallel velocity on the middle plane of the vapor film increased in the outward direction, correspondingly [Fig. 2(b)].

We also calculated the vertical (v) and parallel (u) velocity distributions along the y-axis. Since the vapor is produced at the top of the vapor film (i.e., the bottom of object), the vertical velocity (v) increases from the bottom to the top of the vapor film. However, the parallel velocity (u) assumes a symmetric distribution along the y direction because of the nonslip conditions [Fig. 2(c)]. As the vertical velocity is much smaller than the parallel velocity, the three-dimensional total vapor velocity (U) distribution is dominated by the parallel velocity [Fig. 2(d)].

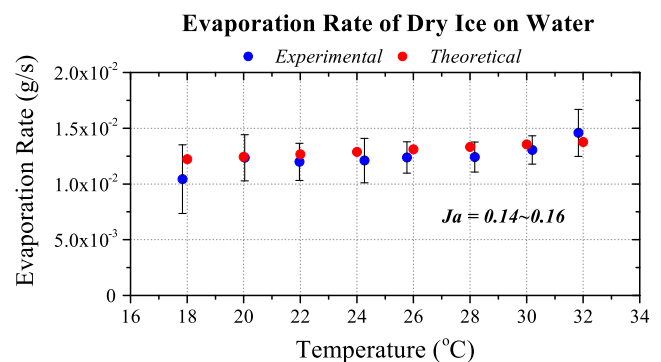


FIG. 3. Theoretical and experimental evaporation rate: blue points (experimental results) and red points (theoretical results).

Referring to Eq. (25), we know that the evaporation rate (M_e) highly depends on the temperature of water (T_s). Therefore, to validate the theoretical analysis in this work, we experimentally measured the evaporation rates of dry ice on the surface of different temperature water and compared them with the theoretical results. The experimental results show that our theoretical calculations (red points) accurately predicted the experimental results (blue points), with the dry ice evaporation rate considerably depending on the temperature of water (Fig. 3). Since the heat flux across the vapor film increases with the increasing water temperature, the evaporation process of dry ice is accelerated.

It is noteworthy that via Eq. (17), we could obtain the dimensionless temperature distribution that only depends on the evaporation Jakob number (Ja) of the object. Consequently, for a given Ja number, the dimensionless temperature distribution across the vapor film is known and the other physical fields of Leidenfrost phenomenon can be quantified. Moreover, the results indicated that if the Ja number is smaller than 0.25, i.e., the evaporation latent heat is more than 4 times the heat capacity of the vapor, the dimensionless temperature distribution can be regarded as linear (criterion: linear correlation coefficient square: $R^2 > 0.999$) (Fig. 4). For instance, through Eq. (16) and corresponding thermal properties, we could obtain that the Leidenfrost systems of a dry ice nub on the water (dry ice: -78.5°C and water: 25°C), a water droplet on a hot surface (water: 99°C and hot surface: 400°C), and an aqueous droplet on the surface of liquid nitrogen (droplet: 25°C and liquid nitrogen: -196°C) have the Ja numbers of 0.15, 0.27, and 1.16, respectively. Hence the temperature distribution across the vapor film in the cases of a dry ice nub on the water and a water droplet on a hot surface can be regarded as linear. However, in the case of an aqueous droplet on liquid nitrogen, it is nonlinear. Therefore, the Ja number is a key indicator of the energy exchange via the evaporation of the object and the heat transfer across the vapor film providing an efficient guide to classify and interpret Leidenfrost phenomena.

We performed the Leidenfrost experiments of liquid nitrogen droplets on the room temperature smooth silicon surface and compared the experimental mass variation with the theoretical prediction with nonlinear temperature and linear temperature hypothesis (Fig. 5). We found that the experimental results (black dots) agreed reasonably well with the nonlinear temperature hypothesis (red line)

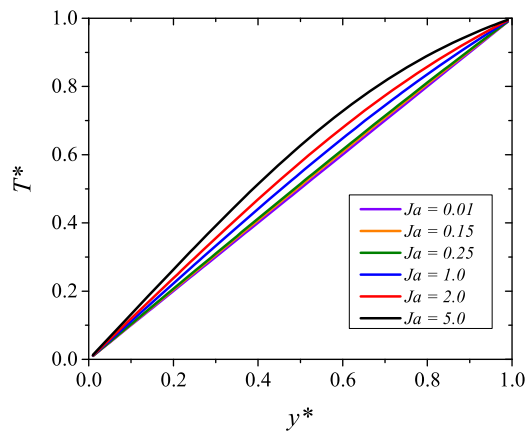


FIG. 4. Jakob number and dimensionless temperature distribution. T^* : dimensionless temperature and y^* : dimensionless position between the substrate and the object in the vertical direction. When the Ja number is smaller than 0.25, the dimensionless temperature distribution can be regarded as linear (linear correlation coefficient square: $R^2 > 0.999$).

rather than the linear one (black line). In other words, the nonlinear temperature distribution does exist in the Leidenfrost phenomenon of the liquid nitrogen droplet on the smooth silicon surface. Considering its Jakob number is beyond 0.25 ($Ja = 1.14$), these results supported our argument regarding the Jakob number's important role in the Leidenfrost phenomenon. With increasing time, the Leidenfrost droplet will become smaller and be close to a spheroid shape as evaporation.²⁷ Thus, the film thickness will be nonuniform which results in the predictive discrepancy becoming larger. Therefore, the discrepancies between theory and experiment after 10 s in Fig. 5 are attributed to the vapor film underneath becoming nonuniform upon evaporation.

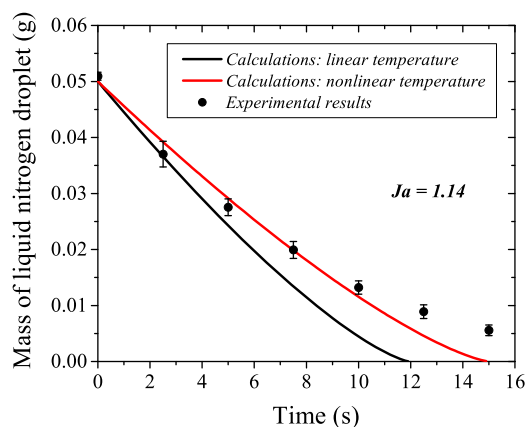


FIG. 5. Mass variation of the liquid nitrogen droplet on the smooth silicon surface at room temperature. Red line: calculated results with nonlinear temperature distribution hypothesis in the current model; black line: calculated results with linear temperature distribution hypothesis which commonly used in previous models; and black dots: experimental results.

V. DISCUSSION

In the current model, we considered convective heat transfer in the vapor film. However, since the temperature difference between the object and the substrate is typically large enough to induce evaporation, radiative heat transfer should be evaluated. In this regard, we simply estimated the radiative transfer assuming blackbody behavior and compared with the conductive heat flux (Q)

$$Q = -k \frac{\partial T}{\partial y} \Big|_{y=\delta}. \quad (29)$$

The results indicated that the conductive heat flux (dry ice on water: $\sim 16\,885 \text{ W/m}^2$ and liquid nitrogen droplet on silicon: $\sim 63\,560 \text{ W/m}^2$) is much higher than the radiative transfer (dry ice on water: $\sim 367 \text{ W/m}^2$ and liquid nitrogen droplet on silicon: $\sim 428 \text{ W/m}^2$) that can thus be ignored.

Meanwhile, the temperature variation of the substrate may influence the heat transfer in the vapor film as well. For example, if the temperature of water decreases due to cooling when the dry ice is placed on the water surface, the temperature distribution in the vapor film and the evaporation of dry ice will be affected. To address this concern, we measured the maximum temperature variation of water by a thermocouple and calculated the respective effect. Based on the definitions of Jakob number [Eq. (16)] and evaporation rate [Eq. (25)], after calculation, we found that the maximum variation of water temperature ($\sim 3 \text{ }^\circ\text{C}$) can only cause $\sim 2.9\%$ variation of the Ja number and $\sim 2.5\%$ variation of the evaporation rate of dry ice, meaning that the temperature distribution and evaporation of dry ice are negligibly affected. At the same time, we measured the temperature of the silicon surface before and after each experiment and we found that the temperature did not have a big range (less than $2 \text{ }^\circ\text{C}$) as the liquid nitrogen droplet is very small, which cannot result in a sufficient cooling of the silicon surface during the period of experiments. Therefore, the effect of substrate temperature variation can be ignored in the context of this work.

It is noteworthy to mention our finding that, in experiments, the dry ice block with the bottom of $50 \text{ mm} \times 10 \text{ mm}$ will immerse into the water when its mass exceeds $\sim 6.9 \text{ g}$. As the levitation force of the dry ice block comes from the pressure force of vapor underneath, this behavior probably attributes to the saturation vapor pressure of dry ice, which sets the upper limit of attainable pressure underneath. At the same time, larger mass leads to larger side surface areas of the dry ice block, which will also affect the bottom vapor release and consequently the vapor pressure underneath. Therefore, our current model is limited by the maximum mass of the levitated object, and the detailed physics will be investigated in the future study.

At the same time, we used the uniform film thickness assumption for simplifying the analysis in this work. In fact, for the Leidenfrost phenomenon of dry ice on a hot surface, since the dry ice is solid and the bottom of dry ice slabs is flat, we believe that the uniform film thickness assumption works well. However, for a liquid droplet, the film thickness in a Leidenfrost system does not always remain uniform. The previous study indicated that a large water droplet (beyond twice the capillary length) in the Leidenfrost state will be flat and but a small one (below the capillary length) will be close to a spheroid.²⁷ Thus, the film thickness under the large droplet will be more uniform than the small one. Therefore, the uniform

film thickness assumption is only appropriate for the liquid droplets whose radii are beyond twice of its capillary length.

Moreover, the temperature distribution inside the vapor film is commonly considered as linear^{27,28,30,35} in previous models. Here, we found that the temperature distribution in the vapor film cannot simply be regarded as linear, and it depends on the Jakob number (Ja) of vapor film. If the Jakob number is lower than 0.25, the temperature distribution can be regarded as linear; otherwise, a nonlinear distribution is more appropriate. We have demonstrated this nonlinear behavior in the Leidenfrost phenomenon of a liquid nitrogen droplet on a smooth silicon surface at room temperature, and we believe that this nonlinear effect can be more remarkable in a hotter silicon surface (higher Ja number). In the future, we will work on adding such experiments into our future studies with a better theoretical model.

It is worth mentioning that our theoretical model will be inaccurate when the object has a tower-like shape ($a, b \ll c$), as the evaporation/sublimation from the free surface will dominate that in the vicinity of the substrate. When the dimension of the levitated object (a or b) is close to the thickness of vapor film (δ), for example, at the later stages of object vaporization, our model will also break down since the lubrication approximate will be no longer applicable.

Although the geometry examined in this theoretical work implies that vapor is released by the object evaporation, it can also be applied to the case where the substrate produces the vapor, for example, an aqueous droplet on the surface of liquid nitrogen²⁶ or a water droplet on a dry ice substrate.²⁵ The same analysis holds by simply moving the origin of the coordinate system to the bottom of the substrate and inverting the y -axis toward the substrate.

We anticipate that the proposed model offers guidelines for investigating Leidenfrost phenomena and even design new Leidenfrost phenomena. Through the theories, we could conveniently determine the temperature distribution in the vapor film of a Leidenfrost phenomenon, as well as design a new Leidenfrost system with linear or nonlinear temperature profile, which has great importance for the Leidenfrost phenomenon related applications, including drag reduction,³⁶ self-propulsion,⁶ and energy conversion.¹¹

VI. CONCLUSION

In this work, we investigated the role of Jakob number in the Leidenfrost phenomena by presenting a theoretical model wherein the vapor film thickness, temperature, pressure, and velocity profiles can be obtained analytically. The dimensionless temperature was found to only depend on the evaporation Ja number of the object. If the Ja number is below 0.25, the temperature distribution can be approximated as linear. The model was validated by examining the evaporation rate of a dry ice slab on the water and the mass variation of a liquid nitrogen droplet on a smooth silicon surface. This study could provide guidance for investigating Leidenfrost phenomena and related applications.

ACKNOWLEDGMENTS

Meng Shi was sponsored by the Chinese Scholarship Council (CSC No. 201506280084) of the Chinese Government. We acknowledge the helpful discussion of Professor Stephen Morris from the Department of Mechanical Engineering, UC Berkeley.

REFERENCES

- B. Gottfried, C. Lee, and K. Bell, "The Leidenfrost phenomenon: Film boiling of liquid droplets on a flat plate," *Int. J. Heat Mass Transfer* **9**, 1167 (1966).
- D. Quéré, "Leidenfrost dynamics," *Annu. Rev. Fluid Mech.* **45**, 197 (2013).
- A. Hashmi, Y. Xu, B. Coder, P. A. Osborne, J. Spafford, G. E. Michael, G. Yu, and J. Xu, "Leidenfrost levitation: Beyond droplets," *Sci. Rep.* **2**, 797 (2012).
- H. Linke, B. J. Alemán, L. D. Melling, M. J. Taormina, M. J. Francis, C. C. Dow-Hygelund, V. Narayanan, R. P. Taylor, and A. Stout, "Self-propelled Leidenfrost droplets," *Phys. Rev. Lett.* **96**, 154502 (2006).
- A. Grounds, R. Still, and K. Takashina, "Enhanced droplet control by transition boiling," *Sci. Rep.* **2**, 720 (2012).
- G. Dupeux, T. Baier, V. Bacot, S. Hardt, C. Clanet, and D. Quéré, "Self-propelling uneven Leidenfrost solids," *Phys. Fluids* **25**, 051704 (2013).
- K. Piroird, B. D. Texier, C. Clanet, and D. Quere, "Reshaping and capturing Leidenfrost drops with a magnet," *Phys. Fluids* **25**, 032108 (2013).
- X. L. Ma, J. J. Lieter-Santos, and J. C. Burton, "The many faces of a Leidenfrost drop," *Phys. Fluids* **27**, 091109 (2015).
- G. Castanet, O. Caballina, and F. Lemoine, "Drop spreading at the impact in the Leidenfrost boiling," *Phys. Fluids* **27**, 063302 (2015).
- F. Moreau, P. Colinet, and S. Dorbolo, "Leidenfrost explosions," *Phys. Fluids* **25**, 091111 (2013).
- G. G. Wells, R. Ledesma-Aguilar, G. McHale, and K. Sefiane, "A sublimation heat engine," *Nat. Commun.* **6**, 6390 (2015).
- R. Abdelaziz, D. Disci-Zayed, M. K. Hedayati, J. H. Pohls, A. U. Zillohu, B. Erkartal, V. S. Chakravadhanula, V. Duppel, L. Kienle, and M. Elbahri, "Green chemistry and nanofabrication in a levitated Leidenfrost drop," *Nat. Commun.* **4**, 2400 (2013).
- S. Saha, M. K. Mandal, H. Nonami, and K. Hiraoka, "Direct analysis of anabolic steroids in urine using Leidenfrost phenomenon assisted thermal desorption-dielectric barrier discharge ionization mass spectrometry," *Anal. Chim. Acta* **839**, 1 (2014).
- H. Kim, B. Truong, J. Buongiorno, and L.-W. Hu, "On the effect of surface roughness height, wettability, and nanoporosity on Leidenfrost phenomena," *Appl. Phys. Lett.* **98**, 083121 (2011).
- J. T. Ok, E. Lopez-Ona, D. E. Nikitopoulos, H. Wong, and S. Park, "Propulsion of droplets on micro- and sub-micron ratchet surfaces in the Leidenfrost temperature regime," *Microfluid. Nanofluid.* **10**, 1045 (2011).
- R. L. Agapov, J. B. Boreyko, D. P. Briggs, B. R. Srijanto, S. T. Retterer, C. P. Collier, and N. V. Lavrik, "Asymmetric wettability of nanostructures directs Leidenfrost droplets," *ACS Nano* **8**, 860 (2013).
- C. Kruse, T. Anderson, C. Wilson, C. Zuhlke, D. Alexander, G. Gogos, and S. Ndao, "Extraordinary shifts of the Leidenfrost temperature from multiscale micro/nanostructured surfaces," *Langmuir* **29**, 9798 (2013).
- H.-m. Kwon, J. C. Bird, and K. K. Varanasi, "Increasing Leidenfrost point using micro-nano hierarchical surface structures," *Appl. Phys. Lett.* **103**, 201601 (2013).
- H. Nair, H. J. Staat, T. Tran, A. van Houselt, A. Prosperetti, D. Lohse, and C. Sun, "The Leidenfrost temperature increase for impacting droplets on carbon-nanofiber surfaces," *Soft Matter* **10**, 2102 (2014).
- I. U. Vakarelski, N. A. Patankar, J. O. Marston, D. Y. Chan, and S. T. Thoroddsen, "Stabilization of Leidenfrost vapour layer by textured superhydrophobic surfaces," *Nature* **489**, 274 (2012).
- M. Shi, X. Ji, S. Feng, Q. Yang, T. J. Lu, and F. Xu, "Self-propelled hovercraft based on cold Leidenfrost phenomenon," *Sci. Rep.* **6**, 28574 (2016).
- Y. S. Song, D. Adler, F. Xu, E. Kayaalp, A. Nureddin, R. M. Anchan, R. L. Maas, and U. Demirci, "Vitrification and levitation of a liquid droplet on liquid nitrogen," *Proc. Natl. Acad. Sci. U. S. A.* **107**, 4596 (2010).
- T. M. Schutzius, S. Jung, T. Maitra, G. Graeber, M. Köhme, and D. Poulikakos, "Spontaneous droplet trampolining on rigid superhydrophobic surfaces," *Nature* **527**, 82 (2015).
- S. D. Janssens, S. Koizumi, and E. Fried, "Behavior of self-propelled acetone droplets in a Leidenfrost state on liquid substrates," *Phys. Fluids* **29**, 032103 (2017).

- ²⁵C. Antonini, I. Bernagozzi, S. Jung, D. Poulikakos, and M. Marengo, "Water drops dancing on ice: How sublimation leads to drop rebound," *Phys. Rev. Lett.* **111**, 014501 (2013).
- ²⁶M. Adda-Bedia, S. Kumar, F. Lechenault, S. Moulinet, M. Schillaci, and D. Vella, "Inverse Leidenfrost effect: Levitating drops on liquid nitrogen," *Langmuir* **32**, 4179 (2016).
- ²⁷A.-L. Bianco, C. Clanet, and D. Quéré, "Leidenfrost drops," *Phys. Fluids* **15**, 1632 (2003).
- ²⁸T. G. Myers and J. P. F. Charpin, "A mathematical model of the Leidenfrost effect on an axisymmetric droplet," *Phys. Fluids* **21**, 063101 (2009).
- ²⁹R. Cantrell, "Gas-film effects in the linear pyrolysis of solids," *AIAA J.* **1**, 1544 (1963).
- ³⁰V. P. Carey, *Liquid-Vapor Phase-Change Phenomena: An Introduction to the Thermophysics of Vaporization and Condensation Processes in Heat Transfer Equipment* (Taylor & Francis, New York, 2008).
- ³¹B. Sobac, A. Rednikov, S. Dorbolo, and P. Colinet, "Self-propelled Leidenfrost drops on a thermal gradient: A theoretical study," *Phys. Fluids* **29**, 082101 (2017).
- ³²J. D. Berry, I. U. Vakarelski, D. Y. C. Chan, and S. T. Thoroddsen, "Navier slip model of drag reduction by Leidenfrost vapor layers," *Phys. Fluids* **29**, 107104 (2017).
- ³³F. Celestini, T. Frisch, A. Cohen, C. Raufaste, L. Duchemin, and Y. Pomeau, "Two dimensional Leidenfrost droplets in a Hele-Shaw cell," *Phys. Fluids* **26**, 032103 (2014).
- ³⁴C. Raufaste, F. Celestini, A. Barzyk, and T. Frisch, "Hole growth dynamics in a two dimensional Leidenfrost droplet," *Phys. Fluids* **27**, 031704 (2015).
- ³⁵G. Bleiker and E. Specht, "Film evaporation of drops of different shape above a horizontal plate," *Int. J. Therm. Sci.* **46**, 835 (2007).
- ³⁶S. Anand and K. K. Varanasi, "Articles and methods for levitating liquids on surfaces, and devices incorporating the same," U.S. patent WO2013188702 (December 19, 2013).